Molecular Crystals and Liquid Crystals
Publication details, including instructions for authors and subscription information:
http://www.tandfonline.com/loi/gmcl20

Synthesis, Electronic Properties, Thermoelectric Power, and Crystal and Band Structures of Unsymmetrical EDOB-EDT-TTF Salts Composed of PF_6^-, AsF_6^-, and SbF_6^- at Various Temperatures

Tomoko Inayoshi [a] & Shiro Matsumoto [a]
[a] Department of Chemistry and Biological Science, College of Science and Engineering , Aoyama Gakuin University , Kanagawa , Japan
Published online: 03 Oct 2013.

To cite this article: Tomoko Inayoshi & Shiro Matsumoto (2013) Synthesis, Electronic Properties, Thermoelectric Power, and Crystal and Band Structures of Unsymmetrical EDOB-EDT-TTF Salts Composed of PF_6^-, AsF_6^-, and SbF_6^- at Various Temperatures, Molecular Crystals and Liquid Crystals, 582:1, 136-153, DOI: 10.1080/15421406.2013.807156

To link to this article: http://dx.doi.org/10.1080/15421406.2013.807156

Mol. Cryst. Liq. Cryst., Vol. 582: pp. 136–153, 2013

ISSN: 1542-1406 print/1563-5287 online
DOI: 10.1080/15421406.2013.807156

Synthesis, Electronic Properties, Thermoelectric Power, and Crystal and Band Structures of Unsymmetrical EDOB-EDT-TTF Salts Composed of PF_6^-, AsF_6^-, and SbF_6^- at Various Temperatures

TOMOKO INAYOSHI* AND SHIRO MATSUMOTO

Department of Chemistry and Biological Science, College of Science and Engineering, Aoyama Gakuin University, Kanagawa, Japan

The synthesis and crystal structure of EDOB-EDT-TTF donor were described. Novel EDOB-EDT-TTF radical salts with different octahedral AsF_6^- and SbF_6^- were prepared. Based on the electrical conductivity measurements, the newly prepared conductive AsF_6 salt underwent a metal-to-semiconductor (MS) transition similar to the previously reported isostructural PF_6 salt. The X-ray analyses of the AsF_6 and SbF_6 salts at various temperatures elucidated their structural characteristics. The AsF_6 salt formed a dimer below 330 K with the formation of an O···H short contact in the intermolecular intradimer along the stacking column. Simultaneous measurements of the thermoelectric power and the resistivity on a single sample were performed for the PF_6, AsF_6, and SbF_6 salts. The MS transition temperatures of these PF_6 and AsF_6 salts were also determined from thermoelectric power data. The band structures and Fermi surfaces for the AsF_6 salts at 293 and 350 K were calculated.

Keywords Band structure; crystal structure; EDOB-EDT-TTF; metal-to-semiconductor transition; octahedral anion salts; thermoelectric power

Introduction

We have previously reported some unsymmetrical EDOB-EDT-TTF charge-transfer complexes and PF_6 and ClO_4 radical salts [1]. The donor molecules in the PF_6 salt were stacked in alternating orientations along the stacking axis. The $(EDOB\text{-}EDT\text{-}TTF)_2PF_6$ salt exhibited high conductivity and a metal-to-semiconductor (MS) transition at around 340 K. The obtained band structure of the PF_6 salt suggested metallic conductive behavior at room temperature. Thus, assuming a doubled period structure, we performed semiempirical unrestricted Hartree-Fock (UHF) calculations with complete neglect of differential overlap (CNDO) approximation. Taking the on-site Coulomb repulsion energy, *U,* into consideration, the energy gap corresponded to the activation energy for the measured conductance.

We then prepared new EDOB-EDT-TTF salts composed of AsF_6^- and SbF_6^- to explore the physical behavior of $(EDOB\text{-}EDT\text{-}TTF)_2X$ salts by varying the octahedron anion X^-. The new AsF_6 salt was found to be isostructural to the PF_6 salt and had a triclinic crystal

*Address correspondence to Tomoko Inayoshi, Department of Chemistry and Biological Science, College of Science and Engineering, Aoyama Gakuin University, 5-10-1 Fuchinobe, Chuo-ku, Sagamihara, Kanagawa 229-8558, Japan. Tel.: +81-042-759-6226; Fax: +81-042-759-6493. E-mail: inayoshi@chem.aoyama.ac.jp

structure, while the new plate SbF_6 salt was not isostructural with the PF_6 and had a monoclinic crystal structure. The AsF_6 salt had a lower MS transition temperature than that of the PF_6 salt, while another SbF_6 salt exhibited semiconductive behavior throughout the temperature range of the conductivity measurements. To clarify the MS transition of these salts, thermoelectric power measurements were also carried out. Thus, a thermoelectric power apparatus was constructed and measurements were performed simultaneously with thermoelectric power and electrical resistivity measurements.

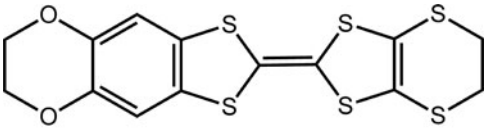

EDOB-EDT-TTF

Picture 1. EDOB-EDT-TTF.

In this paper, we describe crystal structural features for the EDOB-EDT-TTF salts at 90, 293, 330, and 350 K, as well as conductivity, thermoelectric power measurements, and band structures before and after the MS transition. In addition, the synthesis, redox potentials, and crystal structure of the neutral donor are reported.

Experimental

Synthesis of Unsymmetrical EDOB-EDT-TTF Donor

As shown in Scheme 1, the synthesis of EDOB-EDT-TTF was carried out using two synthetic methods: cross-coupling (I) and thermal decomposition (II), resulting in 30% and 27% yields, respectively.

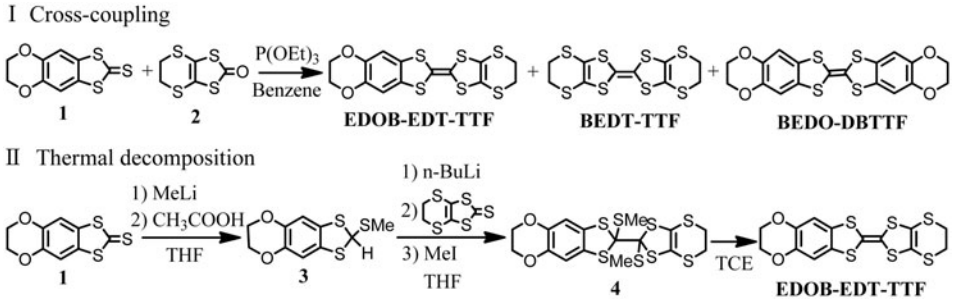

Scheme 1. Synthetic routes of EDOB-EDT-TTF.

I Cross-Coupling Method

To a suspension of **1** (3.0 g, 12 mmol) and **2** (2.5 g, 12 mmol) in dry benzene (40 mL) was added triethylphosphate (30 mL, 130 mmol). The mixture was refluxed for 5 h at 80°C. The resulting orange precipitate was removed by filtration, and the filtrate was purified by silica gel column chromatography using $CHCl_3$/hexane (5:1) as the eluent. The second fraction was collected, and the resulting product was recrystallized using ethyl acetate to afford

EDOB-EDT-TTF as orange crystals (30% yield): mp 260–262°C. ^{1}H NMR ($CDCl_3$): δ 3.30 (4H, s, $-SCH_2$), 4.23 (4H, s, $-OCH_2$), 6.77 (2H, s, ArH). MS (EI) *m*/*z*: 402 (M^+). IR (KBr, ν_{max} cm^{-1}): 1575 (w), 1540 (w), 1478 (s), 1456 (s), 1300 (s), 1376 (m), 1360 (m), 1100 (m), 1063 (s), 908 (m), 895 (m), 854 (m), 772 (w). UV-Vis ($CHCl_3$) λ_{max}, nm: 454, 344, 313, >260. Anal. Calcd for $C_{14}H_{10}O_2S_6$: C, 41.77; H, 2.50; S, 47.78. Found: C, 41.77; H, 2.47; S, 47.74. The product was subsequently subjected to X-ray crystal structure analysis.

II Thermal Decomposition Method

2-(Methylthio)-5,6-ethylenedioxy-1,3-benzodithiole (3). To a solution of **1** (1.03 g, 4.25 mmol) in dry THF (150 mL) at −78°C under nitrogen was added a solution of MeLi (5.1 mL, 6 mmol) dropwise via a syringe. After stirring for 5 h, the mixture was treated with acetic acid (2 mL), and allowed to warm to room temperature. The mixture was combined with water, and the desired compound was extracted using CH_3Cl. The organic layer was dried using $MgSO_4$ and evaporated in vacuo to afford the crude product, which was purified using silica gel chromatography with THF/*n*-hexane (1:3) as the eluent to afford **3** as a colorless oil (0.74 g, 66%). ^{1}H NMR ($CDCl_3$): δ 2.22 (3H, s, $-SCH_3$), 4.21 (4H, s, $-OCH_2$), 5.93 (1H, s, −CH), 6.79 (2H, s, ArH). HRMS (EI) (*m*/*z*): calcd for $C_{10}H_{10}O_2S_2$, 257.9843; found, 257.9718.

Hexathioorthooxalate (4). To a stirred solution of **3** (2.60 g, 10 mmol) in dry THF (120 mL) at −78°C under nitrogen was added *n*-BuLi (6.35 mL, 9.5 mmol) dropwise using a syringe. After stirring for 1 h, 4,5-ethylenedithio-1,3-dithiol-2-thione (2.24 g, 10 mmol) in THF was added dropwise to the mixture, followed by addition of an excess of MeI (1.91 mL, 30 mmol) via a syringe to the mixture after 1 h. After further stirring for 1 h, the solution was treated with portions of 1 mol/dm^3 aq. NH_4Cl. The mixture was allowed to warm to room temperature, and the aqueous layer was extracted with CH_2Cl_2. The organic phase was concentrated and purified using silica gel column chromatography with CH_3Cl/*n*-hexane (1:2) as the eluent to afford **4** as a yellow solid (2.40 g, 45%): mp 207–213°C (dec. 150°C); ^{1}H NMR ($CDCl_3$): δ 2.46 (3H, s, $-SCH_3$), 2.53 (3H, s, $-SCH_3$), 3.25 (4H, m, $-SCH_2$), 4.21 (4H, s, $-OCH_2$), 6.62 (2H, s, ArH). Anal. Calcd for $C_{16}H_{16}O_2S_8$: C, 38.68; H, 3.25. Found: C, 38.56; H, 3.17.

EDOB-EDT-TTF. After refluxing **4** in 1,1,2-trichloroethane (TCE) for 12 h, the crude product was purified by column chromatography with CH_2Cl_2/*n*-hexane (1:1) as the eluent followed by recrystallization from ethyl acetate to yield EDOB-EDT-TTF (27%). ^{1}H NMR and MS data were comparable to those obtained by the cross-coupling method.

Preparation of Radical Salts

New different octahedral AsF_6 and SbF_6 salts were obtained by electrochemical crystallization in distilled TCE under a constant current of 1 μA in a mixture of the donor and the tetrabutylammonium salts of the corresponding anions.

Measurements

General Procedures. ^{1}H NMR spectra were recorded on a JEOL JNM-ECP500 spectrometer with tetramethylsilane (TMS) as an internal standard. Mass spectra were obtained at

70 eV on a JEOL Mstation 700 spectrometer. Electronic absorption spectra were measured on a Shimadzu UV-3101PC spectrophotometer. The stoichiometries of the compounds were determined using elemental analysis. Elemental analyses were carried out either at the Microanalytical Laboratory of Rikagaku Institute (Wako-city, Saitama, Japan) or by using a JM10 elemental analyzer (J-Science Lab, Minami-ku, Kyoto, Japan). Redox potentials were determined on an NGS-301 potentiostat (Nikko Keisoku, Atsugi-city, Kanagawa, Japan). DC electrical resistivities were measured using conventional four- or two-probe methods. Gold wires (25 μm o.d.) were glued to the samples with gold paint (Tokuriki Chemical, no. 8560).

X-ray Crystallography Data. Diffraction data for the donor, AsF_6, and Sb_6 salts were collected with Mo-Kα radiation on a Bruker AXS APEX II CCD diffractometer equipped with a Japan Thermal Engineering Cryosystem DX-CS10KLD at 90, 293, 330, and 350 K. Absorption corrections were applied using the multiscan procedure SADABS. The structures were solved by a direct method using SHELXS-97 [2] and refined by the full-matrix least squares technique. The positions of hydrogen atoms were calculated by assuming a C−H bond length of 0.96 Å and sp^3 conformation of the carbon atoms. Crystallographic information files were deposited with the Cambridge Crystallographic Database for the AsF_6 salts at 90, 293, 330, and 350 K with the reference codes CCDC 819768, 809939, 809703, and 802121, respectively. The files for the SbF_6 salts at 90 and 293 K were also deposited as CCDC 799928 and 799214, respectively. The data for the donor was deposited as CCDC 821631.

Simultaneous Measurements of Thermoelectric Power and Resistivity

The thermoelectric power of the PF_6, AsF_6, and SbF_6 salts was measured using a computer-interfaced system whose schematic diagram is shown in Fig. 1.

A software program for controlling the system was created in LabVIEW by Computer Automation Co. and System Approach Co. By applying different digital signals using a relay and a counter timer, we could perform simultaneous measurements of the thermoelectric power and the two-probe electrical resistivity on a single sample over the entire temperature range [3]. First, by opening the circuit through a Keithley 2002 multimeter attached 2001-Scan scanner card as the relay, the sample voltage (ΔV) between V+ and V− electrodes was measured on a Keithley 2182 nanovoltmeter. The temperature gradient, ΔT, between the two copper plates was measured by another Keithley 2182 nanovoltmeter. The thermoelectric power was determined. Second, after thermal equilibrium was sufficiently reached between the two copper plates, by connecting the circuit through the relay, the voltage was measured by the 2182 nanovoltmeter, while a constant current was supplied to the sample reversing leads to cancel thermal EMFs by a Keithley 220 current source. The two-probe resistance measurement was determined by subtracting these two voltages and averaging. Using the thermoelectric power stage made by MMR Technologies Inc., radical salts and the reference Cu–constantan or Au/Fe–chromel thermocouple wire were glued onto copper plates using gold paint (Tokuriki 8560). A thermal gradient across the sample was applied by heating a 110 Ω chip resistor which was applied from loop 2 of a LakeShore 331S temperature controller. The thermoelectric power was determined from the slope of the line and was calculated as follows: $S = \Delta V / \Delta T$ [4], where ΔT of 15 total points was typically <0.5 K. The changing voltage value was measured at specific, fixed time intervals by 15 points simultaneously using different nanovoltmeters. Therefore, it is necessary to apply synchronously digital signals to two 2182 nanovoltmeters. By using a

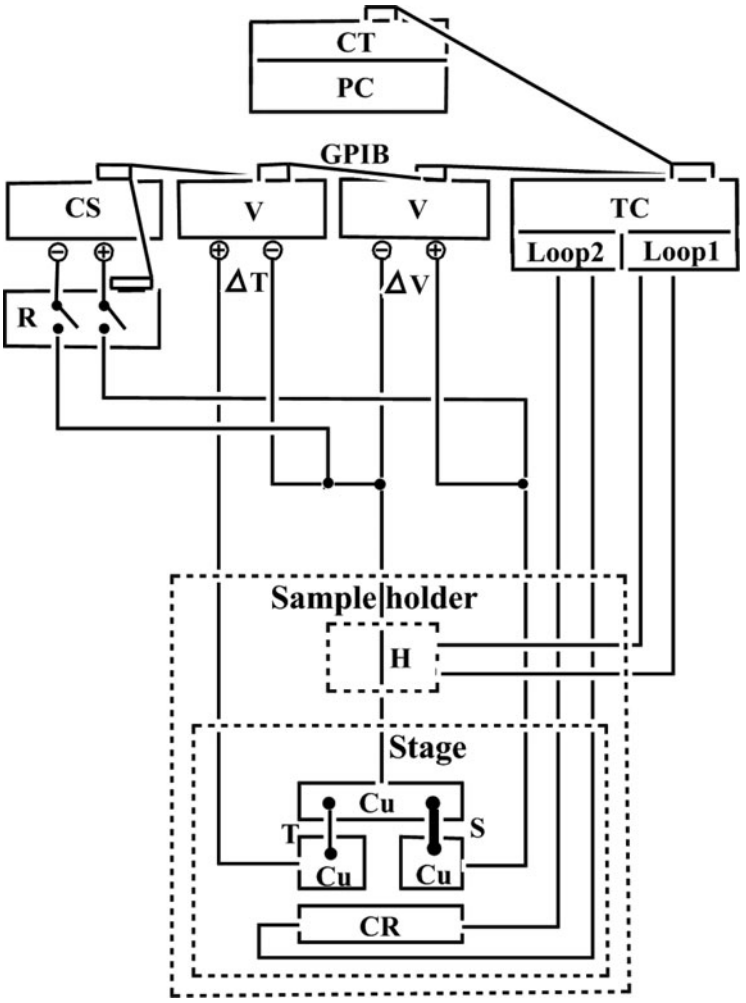

Figure 1. Schematic diagram for the simultaneous measurements of the thermoelectric power and two-probe resistivity. CT; Counter timer 6602, TC; Temperature controller 331S, V; Nanovoltmeter 2182, CS; Current source 220, R; Relay 2002, H; Heater, S; Sample, T; Thermocouple wire, CR; Chip resistor.

National Instruments PCI-6602 counter timer, we could measure 15 points synchronously to determine ΔV and ΔT. It was necessary to subtract the offset drift in order to obtain the absolute thermoelectric power of the samples. At each measurement, the temperature of the sample holder in the cryostat was controlled using loop 1 of the LakeShore 331S temperature controller with a sensor (DT-470). The system was checked by measurements with a Pt standard [5] and TTF-TCNQ complex [6] in the temperature range of 4 to 350 K.

Simultaneous measurements of thermoelectric power and resistivity of the (EDOB-EDT-TTF)$_2$PF$_6$ were also performed on a Quantum Design PPMS Model P670 Thermal Transport System (TTO) in the temperature range of 232–327 K. The crystal, which was glued to the two-probe using bar-shaped copper leads, was mounted on a TTO sample puck.

Table 1. Cyclic voltammetric data

Donor	$E_{1/2(1)}$/V[a]	$E_{1/2(2)}$/V[a]	ΔE/V[b]
EDOB-EDT-TTF	0.53	0.89	0.36
BEDO-DBTTF	0.50	0.90	0.40
BEDT-TTF	0.57	0.90	0.33

[a]$E_{1/2(1)}$ and $E_{1/2(2)}$ redox potentials are for $D^0 \rightarrow D^{+1}$ or $D^{+1} \rightarrow D^{+2}$, respectively; vs. SCE, Pt electrode, 0.1 M Bu_4NClO_4 in CH_2Cl_2, scan rate 200 and 50 mV/s, at 298 K $\pm$ 1.
[b]$\Delta E = (E_{1/2(2)} - E_{1/2(1)})$.

Results and Discussion

Redox Potentials and Crystal Structure of EDOB-EDT-TTF Donor

The redox data obtained from cyclic voltammetry measurements are shown in Table 1.

The EDOB-EDT-TTF donor exhibited two one-electron reversible peaks with a separation of 0.36 V. These peak-potentials had not changed at different scan rates. The ΔE of EDOB-EDT-TTF decreased by 0.04 V compared to BEDO-DBTTF. This indicated that the on-site Coulombic repulsion of EDOB-EDT-TTF decreased.

Crystal and experimental data are shown in Table 2.

The molecular structure of EDOB-EDT-TTF is shown in Fig. 2. EDOB-EDT-TTF is bent in a nonequivalent boat shape [Fig. 2(b)]. The dihedral angles between the central tetrathioethylene plane and the outer ethylenedithio plane are 165° and 166°, respectively (average 166°). In contrast, the tetrathioethylene plane and benzene ring with an ethylenedioxy group are coplanar. The terminal ethylene groups are ordered with an eclipsed conformation. Although two EDOB-EDT-TTF molecules appear to be in a head-to-tail type face-to-face pair, there are no short contacts less than the sum of van der Waals (vdW) radii determined by Bondi [7] within the pair, and the average interplanar distance is 3.59 Å.

The crystal structure of EDOB-EDT-TTF is depicted in Fig. 3. The molecules exhibit some short contacts O(1)···H(13A) (2.597 Å: vdW sum = 2.72 Å) within the molecules of the pair and S(4)···H(13B) (2.851 Å: vdW sum = 3.00 Å) and S(6)···H(5B) (2.876 Å) with the molecules of the adjacent pair. The molecule showed slippage of short contact O(2)···H(8) (2.626 Å) along the transverse direction. The intermolecular distance observed between the S(1)···S(4), S(1)···S(1) and S(5)···S(6) in EDOB-EDT-TTF molecules were 3.643 Å, 3.665 Å, and 3.623 Å, respectively, i.e., more than the vdW sum = 3.60 Å.

Conductivity

The electrical properties of EDOB-EDT-TTF salts are summarized in Table 3.

A new and the previously reported $(EDOB\text{-}EDT\text{-}TTF)_2PF_6$ [1] salts exhibited resistivity decrease with heating (Fig. 4) and showed resistivity minimum at 340 K and then gradual increase up to 350 K.

As shown in Fig. 5, new black plates $(EDOB\text{-}EDT\text{-}TTF)_2AsF_6$ (σ_{RT} = 2.6 Scm^{-1}) exhibited a distinct minimum in resistivity at 315 K confirming an MS transition at this temperature. The semiconductive region (<315 K) showed the activation energy of E_a =

Table 2. Crystallographic data for neutral EDOB-EDT-TTF and its salts at various temperatures

	EDOB-EDT-TTF	PF_6 salt at 298 K	AsF_6 salt at 90 K	AsF_6 salt at 293 K	AsF_6 salt at 330 K	AsF_6 salt at 350 K	SbF_6 salt at 90 K	SbF_6 salt at 293 K
Chemical formula	$C_{14}H_{10}O_2S_6$	$C_{28}H_{20}F_6O_4S_{12}P$	$C_{28}H_{20}F_6O_4S_{12}As$	$C_{28}H_{20}F_6O_4S_{12}As$	$C_{28}H_{20}F_6O_4S_{12}As$	$C_{28}H_{20}F_6O_4S_{12}As$	$C_{28}H_{20}O_4S_{12}SbF_6$	$C_{28}H_{20}O_4S_{12}SbF_6$
Formula weight	402.60	950.23	994.15	994.15	994.15	994.15	1040.99	1040.99
Shape	Orange plate	Black plate	Black plate	Black plate	Black plate	Black plate	Black plate	Black plate
Crystal system	Monoclinic	Triclinic	Triclinic	Triclinic	Triclinic	Triclinic	Monoclinic	Monoclinic
Space group	$P2_1/n$	P-1	P-1	P-1	P-1	P-1	$C2/c$	$C2/c$
a/Å	6.3419 (11)	7.003 (1)	6.8745 (3)	7.0003 (2)	7.0361 (4)	7.0573 (4)	37.8049 (11)	38.1050 (12)
b/Å	21.106 (4)	8.074 (4)	7.9140 (3)	8.0605 (2)	8.0915 (4)	8.1117 (4)	8.2038 (2)	8.3402 (3)
c/Å	11.5743 (19)	16.326 (3)	16.4107 (7)	16.4242 (5)	16.4107 (8)	16.4042 (8)	11.3707 (3)	11.4293 (4)
α/°		76.02 (2)	103.4000	76.0700	76.232 (1)	76.343 (1)		
β/°	95.311 (2)	78.07 (2)	98.3400	78.4100	78.462 (1)	78.489 (1)	103.2300	102.7700
γ/°		81.50 (2)	97.1100	81.4500	81.070 (1)	80.848 (1)		
V/Å^3	1592.6 (4)	871.7 (5)	847.77 (6)	876.23 (4)	883.42 (8)	887.98 (8)	3432.97 (16)	3542.4 (2)
Z	4	1	1	1	1	1	4	4
$D_{calc}(D_{obs})$/gcm^{-3}	1.733 (1.70)	1.81 (1.80)	1.947 (1.85)	1.884 (1.85)	1.869 (1.85)	1.859 (1.85)	2.014 (1.95)	1.952 (1.95)
Diffractometer	Bruker APEX2	Mac Science MXC18	Bruker APEX2	Bruker APEX2	Bruker APEX2	Bruker APEX2	Bruker APEX2	Bruker APEX2
Temperature/K	90	298	90	293	330	350	90	293
Radiation	Mo Kα ($\lambda = 0.71073$Å)	Mo Kα ($\lambda = 0.71073$Å)	Mo Kα ($\lambda = 0.71073$Å)	Mo Kα ($\lambda = 0.71073$Å)	Mo Kα ($\lambda = 0.71073$Å)	Mo Kα ($\lambda = 0.71073$Å)	Mo Kα ($\lambda = 0.71073$Å)	Mo Kα ($\lambda = 0.71073$Å)
Independent reflection	3531 ($I > 3.0\sigma$(I))	3993 ($I > 3.0\sigma(I)$)	2940 ($I > 3.0\sigma(I)$)	3984 ($I > 3.0\sigma(I)$)	3987	4053 ($I > 3.0\sigma(I)$)	3969 ($I > 3.0\sigma(I)$)	4025 ($I > 3.0\sigma(I)$)
R(Rw)	0.0561 (0.2080)	0.0641 (w = 1, 0.0633)	0.0203 (0.1088)	0.0373 (0.1693)	0.0378 (0.1363)	0.0380 (0.1099)	0.0436 (0.1115)	0.0380 (0.0977)
Reference	This study	[1]	This study	This study	This study	This study	This study	This study
g.o.f.	1.786	1.718	1.102	1.600	1.894	1.053	1.020	0.991

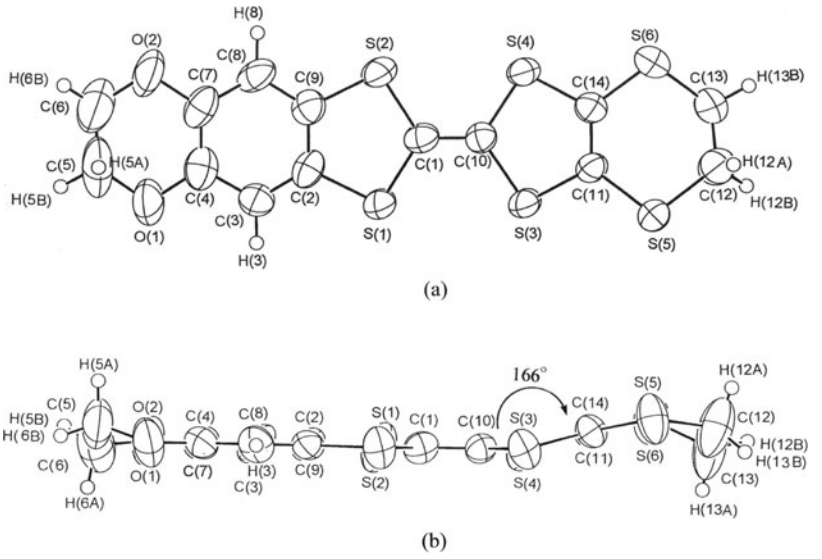

Figure 2. Molecular structure of EDOB-EDT-TTF: (a) front view and (b) viewed along the short axis.

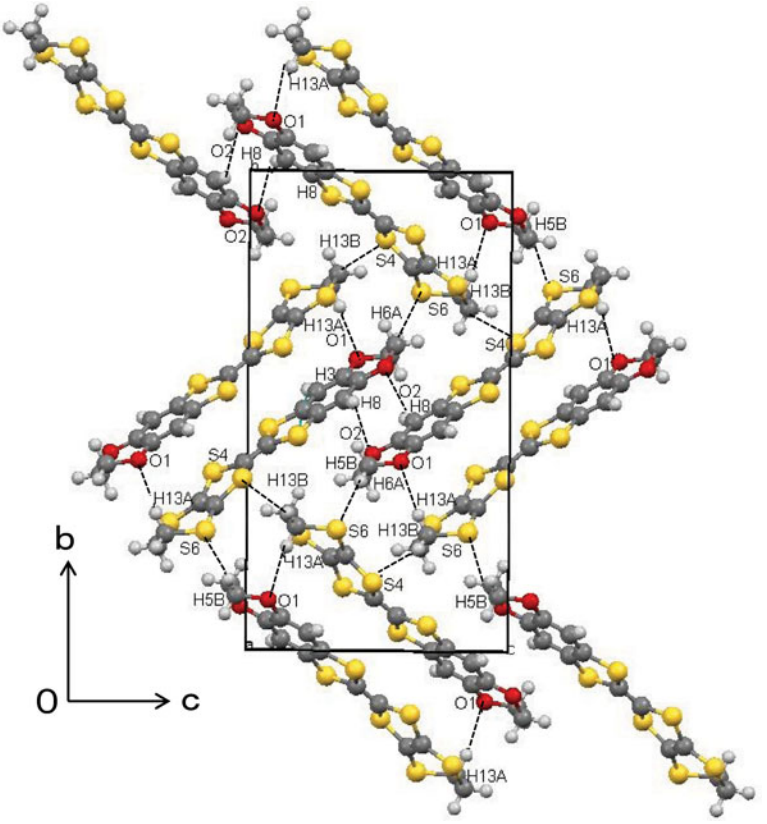

Figure 3. Crystal structure of EDOB-EDT-TTF. The broken lines represent intermolecular O···H and S···H short contacts.

Table 3. Electrical conductivities of EDOB-EDT-TTF salts

Anion	Solvent	Appearance	T_{MS} /K	σ_{RT} /Scm^{-1}	E_a /meV	Reference
PF_6^-	TCE	Black plate	340	1.7×10^{a}	238	[1]
PF_6^-	TCE	Black plate	337	1.0^{b}	167	This study
AsF_6^-	TCE	Black plate	315	2.6^{b}	126	This study
SbF_6^-	TCE	Black plate		$4.4 \times 10^{-2\,b}$	134	This study
SbF_6^-	TCE	Black fine needle		$2.9 \times 10^{-3\,b}$	131	This study

[a]by a four-probe method.
[b]by a two-probe method.

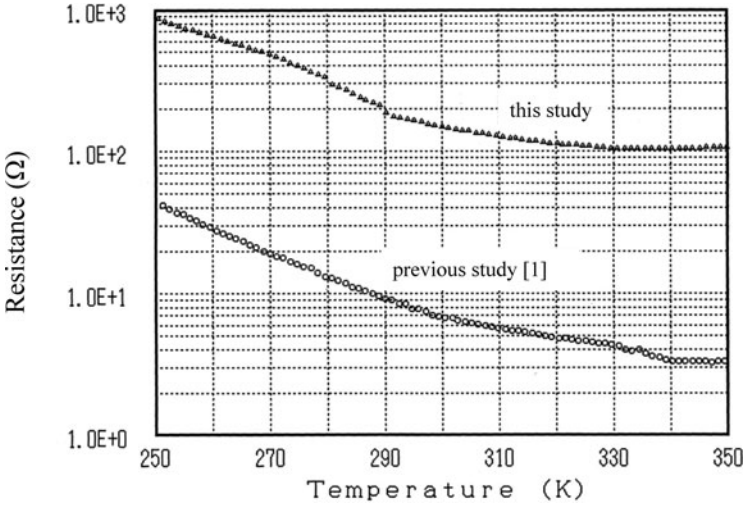

Figure 4. Temperature dependence of resistance of single crystals (EDOB-EDT-TTF)$_2$PF$_6$ in the heating run. Data for the two kinds of crystals are plotted.

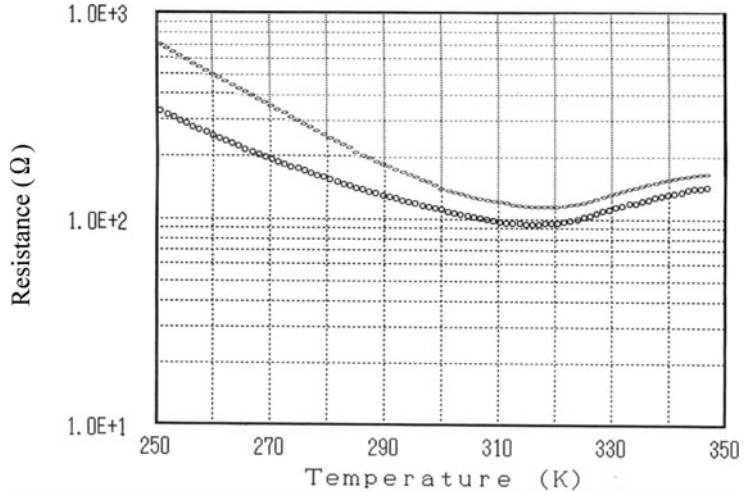

Figure 5. Temperature dependence of resistance of single crystals (EDOB-EDT-TTF)$_2$AsF$_6$ in the heating run. Data for the two kinds of crystals are plotted.

0.126 eV). It was found that the T_{MS} decreased with an increase in the anion size as well as β-(BEDT-TTF)$_2$X (X = PF_6 and AsF_6) [8–10]. The electrical conductivities of the new black plate and fine needle SbF_6 salts at room temperature were 4.4×10^{-2} Scm^{-1} (E_a = 0.134 eV) and 2.9×10^{-3} Scm^{-1} (E_a = 0.131 eV), respectively. The SbF_6 salts behaved as semiconductors from room temperature to 100 K.

Crystal Structure of (EDOB-EDT-TTF)$_2$AsF$_6$

The crystal structure of (EDOB-EDT-TTF)$_2$$AsF_6$ is isostructural to the PF_6 salt and was elucidated at various temperatures (90, 293, 330, and 350 K). The cation layers of EDOB-EDT-TTF molecules and the anion layers of AsF_6 are arranged alternately along the direction of the *c*-axis as shown in Fig. 6.

The EDOB-EDT-TTF molecules are packed head-to-tail in a face-to-face overlapping manner and alternately stacked with a different interplanar along the *b*-axis. This donor packing arrangement is a so-called β-type structure. There are intermolecular short S···S, O···H and S···F contacts less than the vdW sum. Interstack S(1)···S(1) short contacts less than 3.60 Å are observed over the entire temperature range (3.530 Å at 90 K, 3.548 Å at 293 K, 3.555 Å at 330 K, and 3.563 Å at 350 K) and S(3)···S(6) short contacts are found at 90 K (3.536 Å at 90 K, 3.629 Å at 293 K, 3.654 Å at 330 K, and 3.669 Å at 350 K). S···S short contacts are found only between the stacks and not within the stacks. Side-by-side O(2)···H(6B)-C(6) short contacts (2.673 Å at 90 K, 2.647 Å at 293 K, 2.637 Å at 330 K, and 2.634 Å at 350 K) less than the vdW sum in the intermolecular interstack along the *c*-axis are observed over the entire temperature range as shown in Fig. 6(a)(b). O(2)···H(12A)-C(12) short contacts in the intermolecular intrastack along the *b*-axis layers [Fig. 6(a)] can be seen at 90 K (2.440 Å), 293 K (2.610 Å), and 330 K (2.721 Å), but not at 350 K (2.757 Å). Only the O(2)···H(12A)-C(12) short contacts exist in the intermolecular intrastack. The other O(2)···H(6B), S···S and S···F short contacts exist in the intermolecular interstack along the transverse direction. Owing to the effect of dimerization, the distances of O(2)···H(12A)-C(12) at 90, 293, and 330 K are shorter than that at 350 K. Intermolecular S(5)···F(2) short contacts less than the vdW sum (3.27 Å for S···F) between the EDOB-EDT-TTF cations and the hexafluoroarsenate anions are

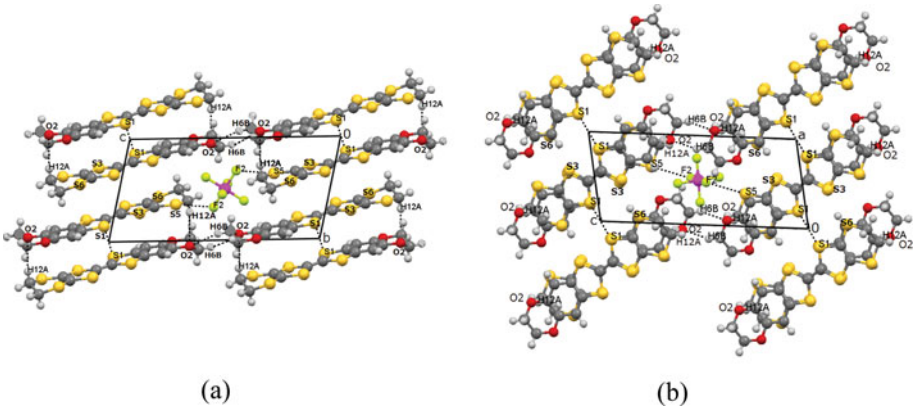

Figure 6. Crystal structure of (EDOB-EDT-TTF)$_2$$AsF_6$ at 293 K showing the short contacts as dashed lines. (a) Projection in the *bc* plane. (b) Projection in the *ac* plane.

Table 4. Bond lengths and dihedral angles of $(EDOB\text{-}EDT\text{-}TTF)_2AsF_6$ salt at various temperatures

	Angstrom			
Bond length	90 K/Å	293 K/Å	330 K/Å	350 K/Å
a	1.367	1.362	1.361	1.361
b	1.742	1.739	1.735	1.737
c	1.742	1.741	1.749	1.738
d	1.357	1.344	1.343	1.344
$\delta = (b+c)-(a+d)$	0.765	0.776	0.777	0.773
b'	1.743	1.739	1.740	1.740
c′	1.752	1.750	1.750	1.749
d′	1.400	1.400	1.397	1.396
		Degree		
Dihedral angle	90 K/°	297 K/°	330 K/°	350 K/°
C14-S6-C13-C12	51.3	47.8	41.6	37.7
C11-S5-C12-C13	43.9	40.4	33.9	30.6
C4-O1-C5-C6	35.8	33.8	32.8	32.4
C7-O2-C6-C5	55.7	53.8	52.2	51.9

observed at 90 K (3.080 Å), 293 K (3.208 Å), and 330 K (3.255 Å), but not at 350 K (3.279 Å). The octahedral anion does not show rotational disorder.

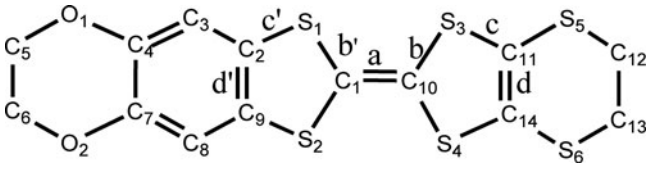

Picture 2. Labelling of the bond lengths in (EDOB-EDT-TTF)2AsF6 salt.

Additionally, the bond lengths and dihedral angles of the ethylenedithio and ethylenedioxy substituents are shown in Table 4. The bond lengths change very little with the variation in temperatures. The dihedral angles of C(14)-S(6)-C(13)-C(12) and C(11)-S(5)-C(12)-C(13) affected by the intermolecular intrastack interaction increase with decreasing temperature, compared with C(4)-O(1)-C(5)-C(6) and C(7)-O(2)-C(6)-C(5). The variation of the bond lengths δ has been used to estimate the degree of charge transfer γ for BEDT-TTF salts [11]. For the EDT site, the γ is estimated to be 0.55 at 293 K. From the central C=C bond length for DBTTF complexes [12], the γ of the EDOB site is estimated to be 0.43 at 293 K. Therefore, the hybridized EDT site has some flexibility.

Crystal Structure of $(EDOB\text{-}EDT\text{-}TTF)_2SbF_6$

$(EDOB\text{-}EDT\text{-}TTF)_2SbF_6$ crystallizes in two forms, plate and needle. The crystal structure of the plate $(EDOB\text{-}EDT\text{-}TTF)_2SbF_6$ is not isostructural to the AsF_6 and PF_6 salts, and belongs to a monoclinic *C*2/c space group, which was elucidated at 90 and 293 K. The

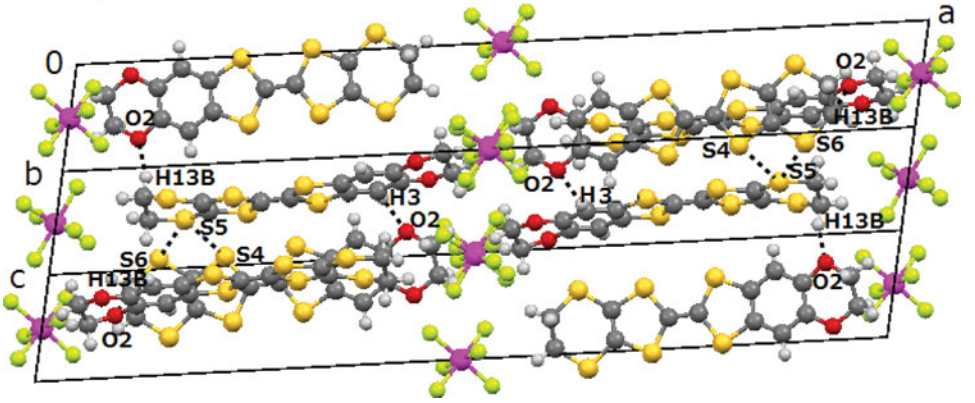

Figure 7. Crystal structure of $(EDOB\text{-}EDT\text{-}TTF)_2SbF_6$ at 293 K showing the intermolecular short O···H and S···S contacts as dotted lines.

needle form is much too small for X-ray crystal structure analysis. The crystal structure of the plate form at 293 K is shown in Fig. 7 and the octahedral SbF_6 anion does not show a disorder.

The molecular arrangement of EDOB-EDT-TTF molecules is quite different from that in $(EDOB\text{-}EDT\text{-}TTF)_2AsF_6$. Two EDOB-EDT-TTF molecules are paired with molecular planes almost parallel, and adjacent pairs are nearly perpendicular to each other. This type of molecular arrangement tends to create two-dimensional networks [13]. However, the SbF_6 salt is a semiconductor. Intermolecular short S···S and O···H contacts are observed, but no S···F contacts are found at 293 K and 90 K. The S···S short contacts at 293 K are between S(4)···S(5) (3.502 Å) and S(5)···S(6) (3.519 Å) as shown in Fig. 7. The S···S short contacts at 90 K are seen at S(3)···S(6) (3.462 Å) and S(5)···S(6) (3.467 Å), and at S(2)···S(3) (3.563 Å) in Fig. 8. The dimerization of two EDOB-EDT-TTF molecules becomes stronger at 90 K. The O···H short contacts are observed at O(2)···H(13B) (2.607 Å) (along the *b*-axis) and O(2)···H(3) (2.470 Å) (along the *c*-axis) at 293 K, and O(1)···H(12A) (2.503

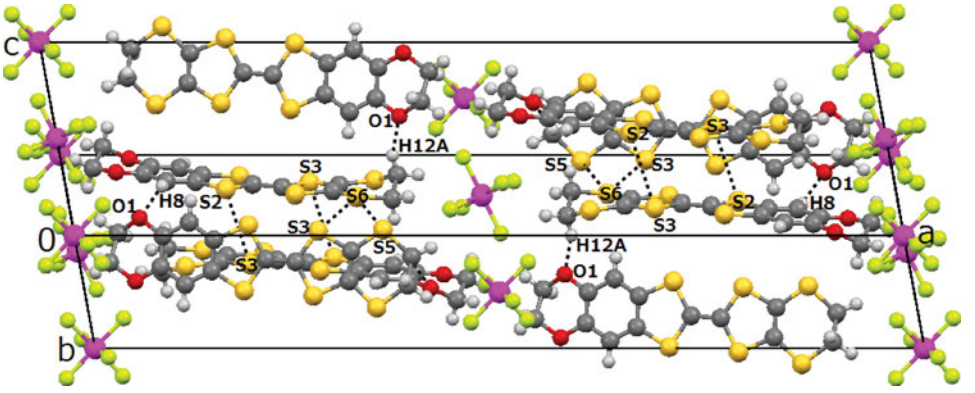

Figure 8. Crystal structure of $(EDOB\text{-}EDT\text{-}TTF)_2SbF_6$ at 90 K showing the intermolecular short O···H and S···S contacts as dotted lines.

Å) (along the *b*-axis) and O(1)···H(8) (2.425 Å) (along the *c*-axis) at 90 K as shown in Figs. 7 and 8, respectively.

Thermoelectric Power

Thermoelectric power measurements were carried out to clarify the MS transition of these salts. The thermoelectric powers of PF_6, AsF_6, and SbF_6 salts were measured in the temperature range of 220–360 K.

A positive thermoelectric power implies a hole-like character of the conduction carriers. The sign of thermoelectric power of the PF_6 salt along the crystal growth axis was positive above 235 K. The value of the thermoelectric power of the PF_6 salt jumps around 340 and 305 K. An inflection of the power curve occurs around 270 K. These jumps and inflection were reproduced for three different samples. The thermoelectric power data of the PF_6 salt shown in Fig. 9 is not clear, however, that of the PF_6 salt was proportional to the absolute temperature down to 320 K, which is characteristic of metallic conduction. Below 320 K, the value of the thermoelectric power dropped gradually, indicating an MS transition around

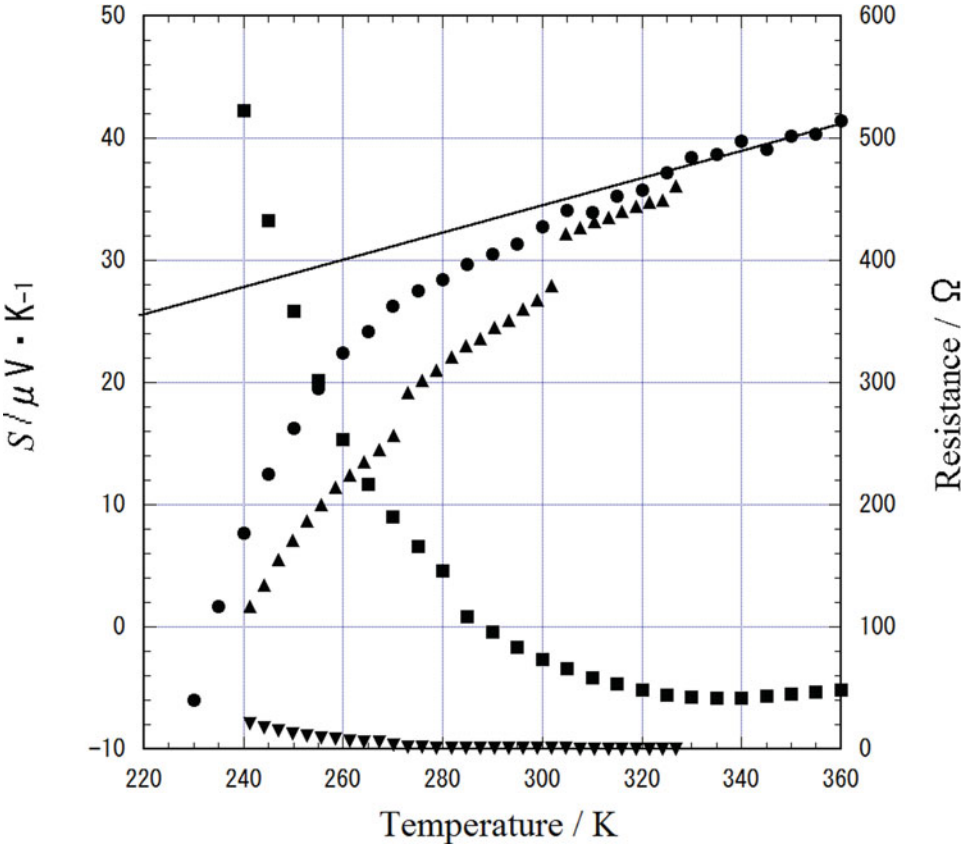

Figure 9. Simultaneous measurements of temperature dependence of thermoelectric power (●) and resistivity (■) of (EDOB-EDT-TTF)$_2$ PF_6 salt. Data of thermoelectric power (▲) and resistivity (▼) were measured by a Quantum Design PPMS in the temperature range of 232–327 K. The solid line extrapolates to zero at $T = 0$ K.

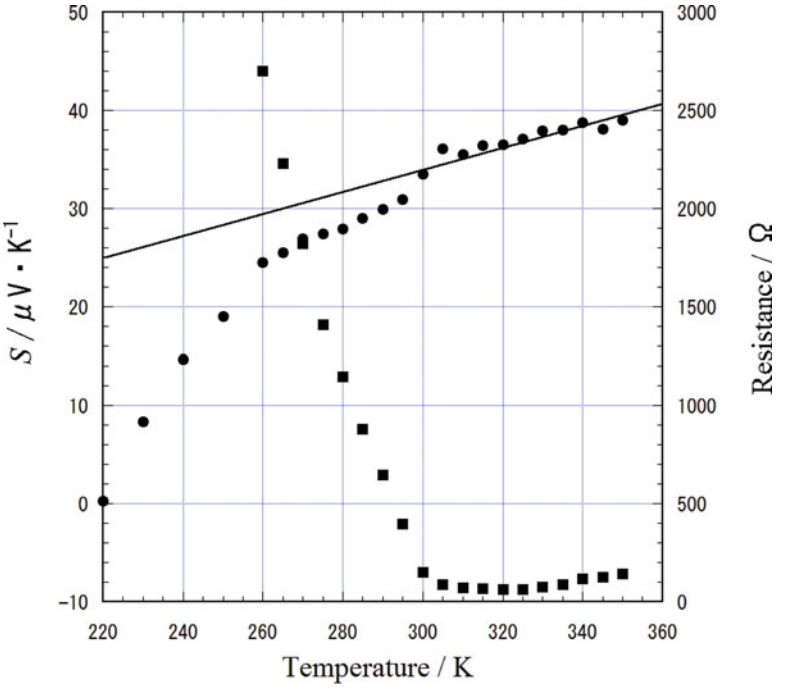

Figure 10. Simultaneous measurements of temperature dependence of thermoelectric power (●) and resistivity (■) of $(EDOB\text{-}EDT\text{-}TTF)_2AsF_6$ salt. The solid line extrapolates to zero at $T = 0$ K.

320 K. These transition temperatures of the PF_6 salt corresponded with the results of the resistivity. The power of the PF_6 salt dropped below 305 K, decreasing rapidly below 270 K.

The thermoelectric power of the AsF_6 salt along the crystal growth axis was linear with temperature down to 310 K, which is characteristic of a metal (Fig. 10). The value of thermoelectric power of AsF_6 seems to jump around 305 K and then drops below 300 K, indicating an MS transition around 310 K. The MS transition temperature observed in the thermoelectric power seems to be slightly lower than that of the conductivity [14]. The power of the AsF_6 salt again showed a rapid decrease below 260 K. An inflection of the power curve was detected around 260 K. These jumps and inflection were reproduced for two different samples. The sign of the thermoelectric power of the AsF_6 salt was positive above 220 K. The thermoelectric power of the AsF_6 salt became negative below 220 K and decreased with decreasing temperature. The MS transition temperatures of the PF_6 and AsF_6 salts observed in the thermoelectric power decreased in the order of 320 K and 310 K. The value of thermoelectric power of the rhombus SbF_6 salt was negative below 335 K and decreased with decreasing temperature, which is a characteristic of a semiconductor (Fig. 11).

Band Structure of the AsF_6 Salt

The band structures of the AsF_6 salt were calculated on the basis of the tight-binding approximation using the intermolecular overlap integrals of the highest occupied molecular orbital (HOMO), which were calculated by the extended Hückel method [15]. X-ray data at

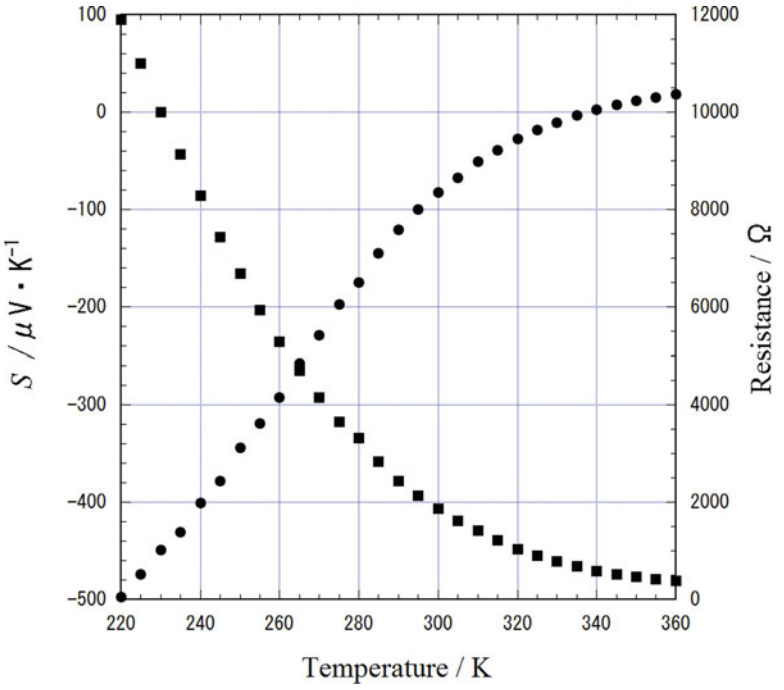

Figure 11. Simultaneous measurements of temperature dependence of thermoelectric power (•) and resistivity (■) of (EDOB-EDT-TTF)$_2$SbF$_6$ salt.

two temperatures, 293 and 350 K, were used. The calculated overlap integrals between the intermolecular are listed in Table 5. Arrangements of donor centers and the intermolecular overlaps in EDOB-EDT-TTF salts viewed onto the *ab* plane are depicted in Fig. 12.

Figure 13 shows the electric band structures and Fermi surfaces of the AsF_6 salt at 293 and 350 K, respectively. The bands of these salts are three-quarters filled and metallic. Short S···S contacts are observed between stacks, not within the stacks. Such a structural feature provides isotropic two-dimensional electronic structures in the Fermi surfaces [16, 17].

Table 5. Intermolecular overlap integrals ($\times 10^{-3}$) of EDOB-EDT-TTF salts

	AsF_6 salt at 293 K	AsF_6 salt at 350 K	PF_6 salt at 293 K [1]
S_a	−3.864	−3.896	−3.886
S_{b1}	12.819	14.467	16.089
S_{b2}	16.414	13.013	12.464
S_{p1}	0.607	5.922	5.545
S_{p2}	5.489	0.605	0.596
S_{q1}	0.058	0.044	0.058
S_{q2}	0.06	0.052	0.056

Symbols S_a∼S_{q2} represent the overlap integrals between donors shown in Fig. 12.

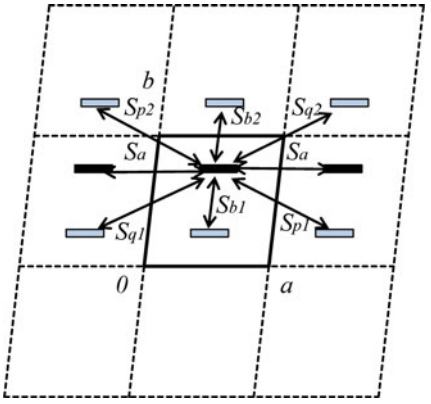

Figure 12. Arrangements of donor centers (▬,▭) and intermolecular overlaps in PF_6 salt at 298 K [1], and AsF_6 salts at 293 K and 350 K viewed onto the *ab* plane.

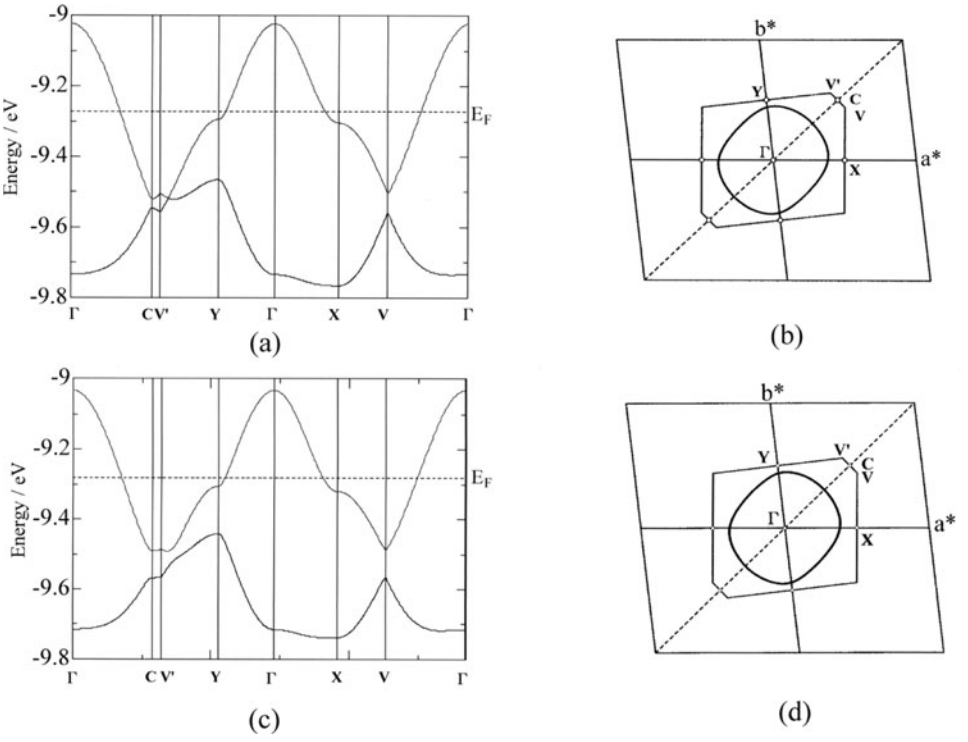

Figure 13. Calculated band structures and corresponding Fermi surfaces of $(EDOB\text{-}EDT\text{-}TTF)_2AsF_6$ salt at 293 K (a, b) and 350 K (c, d).

Conclusion

The synthesis of unsymmetrical EDOB-EDT-TTF donors was accomplished by two methods and the crystal structure of the donor was described. New radical salts with octahedral AsF_6^- and SbF_6^- were prepared by electrochemical oxidation. The crystal structures of the AsF_6 and SbF_6 salts, which form different types of dimers, were determined and analyzed at various temperatures. The crystal structure of the AsF_6 salt was isostructural to the PF_6 salt, but the crystal structure of the plate SbF_6 salt was not. According to electrical conductivity measurements, both the PF_6 and AsF_6 salts exhibited MS transitions at 340 and 315 K, respectively. The resistivities and thermoelectric powers of the EDOB-EDT-TTF salts of PF_6^-, AsF_6^-, and SbF_6- were measured simultaneously on a single sample. Judging from the results of the thermoelectric power measurements, the MS transition temperatures of the PF_6 and AsF_6 salts were around 320 and 310 K, respectively. From the crystal structure analysis in the AsF_6 salt, the distances of intermolecular O(2)···H(12A)-C(12) along the stacking *b*-axis at 350, 330, 293, and 90 K decrease in that order by the dimerization. The formation of dimers results in the semiconductor transition. The short S···S contacts were found only between the stacks and not within the stacks. They provided an isotropic two-dimensional electric structure in the Fermi surfaces. The two-dimensional electric structure derived from the β-type arrangement is not so stable against the packing modification [17]. The MS transition is associated with some structural transition.

Acknowledgments

The authors wish to thank Dr. Takehisa Maeda and Mr. Kennchi Yamashita of Computer Automation Co. and Mr. Nobuo Niwa of System Approach Co. for programming the LabVIEW thermoelectric power measurement system and Mr. Atsuhiro Urata of International Servo Data Co. for the thermoelectric power apparatus.

References

[1] Inayoshi, T., Matsumoto, S., & Ono, I. (2003). *Synth. Met*., *345*, 133.
[2] Sheldrick, G. M. (1997). SHELXS-97 and SHELXL-97, Program for Crystal Structure Solution. University of Göttingen, Germany.
[3] Kim, G. T., Park, J. G., Lee, J. Y., Yu, H. Y., Suh, E. S., Ha, Y. S., & Park, Y. W. (1998). *Rev. Sci. Instrum*., *63*, 3705.
[4] Park, Y. W. (1991). *Synth. Met*., *45*, 173.
[5] Barnard, R. D. (1972). *Thermoelectricity in Metals and Alloys*, Taylor & Francis: London, Chapter 2, p. 49.
[6] (a) Kwak, J. F., Chaikin, P. M., Russel, A. A., Garito, A. F., & Heeger, A. J. (1975). *Solid State Commun*., *16*, 729. (b) Chaikin, P. M., Greene, R. L., Etemad, S., & Engler, E. (1976). *Phys. Rev. B*, *13*, 1627.
[7] The van der Waals radii employed in this paper are as follows: C 1.70, H 1.20, N 1.55, O 1.52, S 1.80, F 1.47; Bondi, Å. A. (1964). *J. Phys. Chem*., *68*, 441.
[8] Kobayashi, H., Mori, T., Kato, R., Kobayashi, A., Sasaki, Y., Saito, G., & Inokuchi, H. (1983) *Chem. Lett*., *12*, 581.
[9] Laversanne, R., Amiell, J., Delhaes, P., Chasseau, D., & Hauw, C. (1985). *Mol. Cryst. Liq. Cryst*., *119*, 405.
[10] Senadeera, G. K. R., Kawamoto, T., Mori, T., Yamaura, J., & Enoki, T. (1998). *J. Phys. Soc. Jpn*., *67*(12), 4193.
[11] Guionneau, P., Kepert, C. J., Bravic, G., Chasseau, D., Truter, M. R., Kurmoo, M., & Day, P. (1997). *Synth. Met*., *86*, 1973.

[12] Emge, T. J., Wiygul, F. M., Chappell, J. S., Bloch, A. N., Ferraris, J. P., Cowan, D. O., & Kistenmacher, T. J. (1982). *Mol. Cryst. Liq. Cryst.*, *87*, 137.
[13] Ishiguro, T., Yamaji, K., & Saito, G. (1998). *Organic Superconductors,* 2nd ed., Springer: Berlin, Chapter 5.
[14] Kikuchi, K., Saito, K., & Ikemoto, I. (1988). *Synth. Met.*, *27*, B269.
[15] Mori, T., Kobayashi, A., Sasaki, Y., Kobayashi, H., Saito, G., & Inokuchi, H. (1984). *Bull. Chem. Soc. Jpn.*, *57*, 627.
[16] Wosnitza, J. (1996). *Fermi Surfaces of Low-Dimensional Organic Metals and Superconductors*, Springer: Berlin, p. 34.
[17] Kagoshima, S., Kato, R., Fukuyama, H., Seo, H., & Kino, H. (1999). In: P. Bernier, S. Lefrant, & G. Bidan (Eds.), *Advances in Synthetic Metal: Twenty Years of Progress in Science and Technology*, Elsevier: Amsterdam, Chapter 4, p. 266.